Arc ubiquitination regulates endoplasmic reticulum-mediated Ca^{2+} release and CaMKII signaling

Ghane MA[1,2], Allen ZD[1,2], Miller CL[3], Dong B[3,4], Fang N[3], Yang JJ[3], Mabb AM*[1,2]

[1]Georgia State University, Neuroscience Institute, Atlanta, Georgia, United States of America

[2]Georgia State University, Center for Behavioral Neuroscience, Atlanta, Georgia, United States of America

[3]Georgia State University, Department of Chemistry, Atlanta, Georgia, United States of America

[4]University of Arkansas, Department of Chemistry and Biochemistry, Fayetteville, Arkansas, United States of America

*** Correspondence:**

Dr. Angela M. Mabb

amabb@gsu.edu

Keywords: Arc, CaMKII, ubiquitin, endoplasmic reticulum, calcium signaling, long-term depression, synaptic plasticity

Abstract

Synaptic plasticity relies on rapid, yet spatially precise signaling to alter synaptic strength. Arc is a brain enriched protein that is rapidly expressed during learning-related behaviors and is essential for regulating metabotropic glutamate receptor-mediated long-term depression (mGluR-LTD). We previously showed that disrupting the ubiquitination capacity of Arc enhances mGluR-LTD; however, the mechanism by which this occurs and its consequences on other mGluR-mediated signaling events is unknown. Here we show that disrupting Arc ubiquitination on key amino acid residues leads to derangements in Ca^{2+} release from the endoplasmic reticulum (ER) during pharmacological activation of Group I mGluRs. These alterations were observed in all neuronal subregions except secondary branchpoints. Deficits in Arc ubiquitination increased Arc self-association and enhanced its interaction with calcium/calmodulin-dependent protein kinase IIb (CaMKIIb) and constitutively active forms of CaMKII. Notably, these interactions were also excluded at secondary branchpoints. Finally, disruptions in Arc ubiquitination were found to increase Arc interaction with the integral ER protein Calnexin. These results suggest a previously unknown role for Arc ubiquitination in the fine tuning of ER-mediated Ca^{2+} signaling that is needed for mGluR-LTD, which, in turn, regulates CaMKII-dependent regulation of Arc.

Introduction

Synaptic plasticity relies on rapid, yet spatially precise signaling to appropriately alter synaptic strength. Metabotropic glutamate receptor-mediated long-term depression (mGluR-LTD) is a protein synthesis-dependent form of plasticity that is mediated by activation of G_q-coupled receptor pathways, activating endoplasmic reticulum (ER)-bound inositol triphosphate receptors (IP_3Rs) to allow Ca^{2+} efflux, which is canonically associated with α-amino-3-hydroxy-5-methyl-4-isoxazolepropionic acid (AMPA) receptor endocytosis (Abe et al., 1992; Aramori and Nakanishi, 1992; Palmer et al., 1997; Snyder et al., 2001; Wilkerson et al., 2018). It is well established that neurons contain highly complex continuous ER networks that extend throughout different subregions, with ER morphology increasing in complexity at dendritic branchpoints and $[Ca^{2+}]_{ER}$ varying at different compartments of the ER (Terasaki et al., 1994; Spacek and Harris, 1997; Cui-Wang et al., 2012; Krijnse-Locker et al., 2017). Furthermore, the distribution of IP_3Rs themselves vary throughout the neuron, with higher levels found at neuronal proximal regions (Sharp et al., 1993; Blaustein and Golovina, 2001). While the significance of these various gradients for neuronal function and behavioral output are not completely understood, it is hypothesized that they offer an additional layer of local protein synthesis and trafficking regulation to various regions of the neuron.

Activity-regulated cytoskeleton-associated protein (Arc) is vital for numerous forms of synaptic plasticity that include mGluR-LTD (Lyford et al., 1995; Chowdhury et al., 2006; Plath et al., 2006; Shepherd et al., 2006; Beique et al., 2011; Korb and Finkbeiner, 2011; Jenks et al., 2017; Pastuzyn and Shepherd, 2017; Mabb and Ehlers, 2018;

Newpher et al., 2018). Arc induction is spurred by diverse learning and memory related behaviors, including spatial memory acquisition, consolidation, and retrieval (Guzowski et al., 1999; Ramirez-Amaya et al., 2005; Plath et al., 2006; Bramham et al., 2008; Nakayama et al., 2015). Importantly, Arc is rapidly degraded, largely through proteasome- and lysosome-dependent processes (Rao et al., 2006; Yan et al., 2018). Arc can be degraded by ubiquitination of two tandem lysine residues (268/269) catalyzed by the E3 ubiquitin ligase TRIAD3A/RNF216, which induces proteasome-dependent degradation of Arc (Mabb et al., 2014). We previously mutated these tandem ubiquitination Lysine sites 268/269 to Arginine (ArcKR), which led to alterations in AMPA receptor trafficking, enhanced mGluR-LTD, and selective deficits in spatial reversal learning that include a bias in utilization of inefficient search strategies (Wall et al., 2018).

Calcium/calmodulin-dependent protein kinase II (CaMKII) is another hub of synaptic plasticity known to be essential for learning and plasticity (Coultrap et al., 2014; Murakoshi et al., 2017; Rossetti et al., 2017; Bayer and Schulman, 2019). CaMKII activity is tightly regulated by extra- and intracellular Ca^{2+} dynamics, resulting in autophosphorylation at specific threonine residues that determine activity states (Glazewski et al., 2000; Elgersma et al., 2002; Gillespie and Hodge, 2013). Previous work has also shown that CaMKII plays a role in mGluR-LTD (Mockett et al., 2011; Cook et al., 2022) and, interestingly, there is evidence from classical work that suggests dysregulation of CaMKII and resulting enhancement of LTD lead to alterations in spatial search strategies (Bach et al., 1995).

Arc interacts with both forms of CaMKII (Donai et al., 2003; Okuno et al., 2012) and this regulation is believed to recruit Arc to different subdomains that include inactive synapses, with initial findings showing greater affinity for the inactive beta isoform of CaMKII (CaMKIIb) (Okuno et al., 2012). Recent evidence indicates that CaMKII phosphorylates the GAG domain of Arc, promoting Arc oligomerization and increasing the magnitude of mGluR-LTD (Zhang et al., 2019; Zhang and Bramham, 2020).

Given the importance of Arc mRNA and protein localization to highly specific regions of the neuron and its diverse functions (Steward et al., 1998; Moga et al., 2004; Chowdhury et al., 2006; Peebles et al., 2010; Okuno et al., 2012), it remains to be seen whether the confluence of ER-Ca^{2+} gradients, CaMKII regulation of Arc localization and function, and the temporal dynamics of Arc expression could act as a mechanism for mGluR-LTD regulation and its resulting functional outputs. Here, we used the ArcKR model to investigate this possibility. We found that deficits in Arc ubiquitination on K268/269 sites leads to aberrations in ER-Ca^{2+} relase upon chemical induction of mGluR-LTD in hippocampal neurons. This alteration was observed in all neuronal subregions except for secondary branchpoints. ArcKR was also found to have increased self-association and enhanced binding with activated versions of CaMKII compared to wildtype (WT) Arc. Furthermore, Arc-CaMKII colocalization was variable throughout neuronal regions, which was disrupted in ArcKR neurons. Collectively, our findings suggest a possible role for Arc ubiquitination in regulating ER Ca^{2+} dynamics, self-association, and regulation of CaMKII.

Materials and Methods

Animals

All animal care and use were carried out in accordance with the *National Institutes of Health Guidelines for the Use of Animals* using protocols approved by the Georgia State University Institutional Animal Care and Use Committee.

Cell culture

Primary hippocampal neuron cultures were generated from postnatal day 0-1 WT and ArcKR littermates as previously described (Wall et al., 2018). Neurons were grown on poly-d-lysine (0.1 mg/mL)-coated 6-well plates (9.6 cm^2) at a density of 300,000 cells/well for Western blotting applications; on PDL-coated (1 mg/mL) coverslips (12 mm diameter) in 24-well dishes (3.5 cm^2) at a density of 75,000 cells/dish for immunocytochemistry (ICC) applications; and on PDL-coated (1 mg/mL) coverslips (24 mm x 60 mm) in 60 mm culture plates at a density of 75,000 cells/dish for live imaging experiments. Neurons were maintained in neuronal feeding media (Neurobasal media, ThermoFisher Scientific) containing 1% GlutaMAX (ThermoFisher Scientific), 2% B-27 (ThermoFisher Scientific), 4.8 µg/mL 5-Fluoro-2'-deoxyuridine (Sigma), and 0.2 ug/mL Gentamicin (Sigma) and fed by replacing half of the feeding media with fresh, pre-warmed neuronal feeding media every 3-4 days until used for experiments as described below.

HEK293 cells (ATCC) were seeded and maintained using standard procedures in Dulbecco's modified Eagle's medium (DMEM; Corning #10-017-CV) containing 10% FBS and 1% penicillin-streptomycin (ThermoFisher).

HILO ER calcium imaging

Cultured primary hippocampal neurons were transfected with G-CatchER$^+$ using Lipofectamine 2000 reagent (ThermoFisher Scientific) with a modified version of the manufacturer's protocol as previously described (Reddish et al., 2021) at days in vitro (DIV) 11-12. Neurons were imaged at DIV 12-14.

G-CatchER$^+$-transfected neurons were transferred to pre-warmed (37°C) artificial cerebrospinal fluid (ACSF; 124 mM NaCl, 3 mM KCl, 2 mM CaCl2, 2 mM MgCl2, 10 mM HEPES, 10 mM D-Glucose, pH 7.4). A G-CatchER$^+$-positive neuron was identified and a signal was acquired at baseline. Drugs were pre-warmed to 37°C (100 μM (S)-3,5-DHPG (DHPG) (Tocris) in ACSF or 50 μM ionomycin (ThermoFisher Scientific) in ACSF modified with 10 mM Ca^{2+}) and then washed in manually using a syringe that was connected via tubing to the imaging chamber. For DHPG experiments, drug was washed out with pre-warmed ACSF.

For highly illuminated laminated optical sheet (HILO) microscopy, a fiber-coupled 488 nm laser (Oxxius) was first collimated and then focused at the back focal plane of a 100X oil TIRF objective (N.A. 1.49, Nikon) using an achromatic lens with a focal length of 200 mm (Thorlabs) as previously described (Deng et al., 2021; Reddish et al., 2021). The position of the focused laser at the back focal plane of the objective was controlled by a 2D translational stage (Thorlabs). By laterally shifting the laser beam, the incident angle of laser beam at the interface of coverslip and cell can be easily controlled. To achieve HILO imaging, the incident angle of laser beam at the interface was adjusted to the sub-critical angle of total internal reflection where a thin optical light sheet was refracted into cells and excited the fluorophores within a few tens of micrometers from the coverslip surface. Laser power was kept consistent at 0.7 mW to minimize photobleaching. Images were acquired with a highly sensitive electron multiplying charge-coupled device (EMCCD) camera (Andor Ixon Ultra 888) at a rate of 2 frames/sec.

Live cell images were analyzed as previously described (Deng et al., 2021; Reddish et al., 2021) in ImageJ (NIH) by manually drawing a region of interest around clearly

visible sub-regions of neurons (soma, primary branchpoints (PB)s, primary dendrites (PD)s, secondary branchpoints (SB)s, and secondary dendrites (SD)s) and fluorescence traces extracted. Raw pixel values were normalized to the average baseline fluorescence to generate a profile plot. Rigid motion correction was applied in cases where the neuronal subregion drifted partially or entirely out of the drawn regions of interest using the Rigid Registration ImageJ plugin. Videos were carefully inspected to verify cell health and data discarded in cases of clear cell morphological changes that indicated cell death (severe punctation, shriveling, or massive changes in fluorescence that were not associated with drug treatment). Basal $[Ca^{2+}]_{ER}$ was calculated from the traces of the ionomycin-treated neurons using a previously described method (de Juan-Sanz et al., 2017; Reddish et al., 2021).

Immunocytochemistry

Cultured primary hippocampal neurons on coverslips were fixed at DIV 12-14 with 4% paraformaldehyde and 4% sucrose in phosphate-buffered saline (PBS) at 37°C, washed with PBS, permeabilized with 0.1% Triton X-100 in PBS for 15 min at room temperature, and blocked with 10% normal goat serum (Gibco #16-210-072) for 1 hr at 37°C. Cells were then incubated with primary antibodies (rabbit anti-Arc (Synaptic Systems #156003; 1:500); rabbit anti-CaMKIIα/β (Abcam #ab52476; 1:250)) overnight at 4°C in 3% normal goat serum in PBS, washed with PBS, and incubated with secondary antibodies (donkey anti-mouse AlexaFluor 568 (Invitrogen #A10037; 1:1000); goat anti-rabbit AlexaFluor 488 (Life Tech #A11008; 1:1000)) for 1 hr at room temperature. After a final washing with PBS, coverslips were mounted onto slides with Fluorogel (GeneTex) or Vectashield Vibrance (Vector Laboratories) hardening mounting media with DAPI.

Neurons were imaged on a Zeiss LSM 700 confocal microscope using a 63X oil immersion objective lens (NA 1.4, Zeiss #420782-9900-000). Raw z-stack images (step size 0.27 μm) were analyzed using ImageJ (NIH) by manually drawing regions of interest around clearly visible sub-regions of neurons (soma, PBs, PDs, SBs, and SDs)

and the integrated density was measured. All parameters related to acquisition were kept constant for all images within a given dataset. For colocalization analysis, the Coloc 2 plugin (bisection threshold regression) was used to calculate above-threshold pixel-pixel Pearson's correlation coefficients between channels.

Western blotting

Cultured primary hippocampal neurons were harvested by briefly washing the plates in Dulbecco's phosphate buffered saline (Gibco #14190144) and removed from the plate using a cell scraper (Corning #3010) and pelleted by centrifugation. Cell pellets were lysed in radioimmunoprecipitation assay (RIPA) buffer (150 mM NaCl, 50 mM Tris-HCl, 1% v/v Nonidet P-40, 0.05% sodium deoxycholate, 0.01% SDS) for 30 min on ice. For primary hippocampal neuron cultures, the entire cell lysate was used without assaying protein content due to low protein content and small volume. Following separation by SDS-PAGE, proteins were transferred to a nitrocellulose membrane (0.45 μm pore size, Bio-Rad). Membranes were blocked with Intercept TBS blocking buffer (LI-COR) overnight at 4°C and then incubated with primary antibodies (Arc, Synaptic Systems #156003, 1:1000; CaMKII, Abcam #ab52476, 1:1000; CaMKII p-Thr286 p-Thr287 Novus Biologicals #NB110-96896, 1:1,000; GAPDH, GeneTex #GTX627408, 1:1250) in a solution containing 1:1 blocking buffer:1% Tween-20 in tris-buffered saline (TBST) overnight at 4°C. After washing with TBST, membranes were incubated with secondary antibodies (IRDye Goat anti-Mouse 680RD, LI-COR #926-68070, 1:15,000, IRDye Goat anti-Rabbit 800CW, LI-COR #926-32211, 1:15,000) in 1:1 blocking buffer:TBST for 1 hr at room temperature. Membranes were imaged on a LI-COR Odyssey CLx scanner (low scan quality, 163 μm scan resolution, auto channel intensities) and resulting images were analyzed using the gel analysis tool in ImageJ (NIH). For images where high background was present, background subtraction was performed on the whole channel using the Subtract Background tool in ImageJ with a rolling ball radius of 20-50 pixels.

Co-immunoprecipitation

HEK293 cells were seeded on 6-well plates and transfected with pRK5-myc-Arc, pRK5-myc-ArcKR, pEGFP-Arc, pEGFP-ArcKR, pCAG-mEGFP-CaMKIIα, and/or pCAG-mEGFP-CaMKIIβ, pCAG-mEGFP-CaMKIIα T286A, pCAG-mEGFP-CaMKIIα T286D, pCAG-mEGFP-CaMKIIβ T287A, pCAG-mEGFP-CaMKIIβ T287D, and/or mVenus-Calnexin (Addgene #56324) (CaMKII plasmids were a kind gift from Dr. Ulli Bayer at the University of Colorado Medicine (Bayer et al., 2006b)) using Lipofectamine 2000 or Lipofectamine 3000 reagent (ThermoFisher Scientific) following the manufacturer procedure. After allowing constructs to express overnight, cells were harvested and lysed in immunoprecipitation (IP) buffer (20 mM Tris-HCl, 3 mM EDTA, 3 mM EGTA, 150 mM NaCl, 1% Triton X-100, 1 mM DTT, pH 7.4) containing protease and phosphatase inhibitors (0.1 mM phenylmethylsulfonyl fluoride, 1 μM leupeptin, 0.15 μM aprotinin, and 1:2000 Halt phosphatase inhibitor cocktail (ThermoFisher Scientific #78420)) for 30 min on ice. After centrifugation (14,000 rpm, 25 min, 4°C), lysate protein concentration was determined using a Pierce 660 assay (ThermoFisher). 10 μg of protein was used for subsequent steps, with 1 μg of protein (10%) reserved for input control. Lysates were incubated with 0.5 μg/mL monoclonal mouse anti-myc antibody (Santa Cruz Biotech #sc-40) for 1 hr at 4°C. 25 μL of pre-equilibrated GammaBind Sepharose beads (Cytiva) were then added and samples tumbled overnight at 4°C. Samples were washed with IP buffer and proteins were eluted from beads using SDS sample buffer (Li-Cor #928-40004) with heating at 45°C for 5 min. Subsequently, beads were pelleted by centrifugation (15,000 rpm for 2 min) and the supernatant containing protein was separated using SDS-PAGE, transferred to a nitrocellulose membrane, and immunoblotting proceeded as described above using anti-GFP (Fisher #NB600308, 1:1000) and polyclonal goat anti-myc (Bethyl/ThermoFisher #A190-104A, 1:1000) primary antibodies. For quantification, GFP-tagged co-immunoprecipitated protein band intensities were normalized to the immunoprecipitated myc-tagged protein, which served as an internal control of IP efficiency.

Protein purification

Purification of His-tagged WT Arc and ArcKR was carried out by a third-party company (GenScript Biotech, New Jersey, USA) using their HD transient expression of recombinant protein – gold system. Briefly, the sequences for ArcWT and ArcKR were synthesized and cloned into the pcDNA3.4 target vector using the EcoRI and HindIII restriction sites. Plasmids were then transfected into the HD 293F cell line for expression. Protein was purified using HisTrap FF Crude (Cytiva) purification columns and eluted in PBS, pH 7.2. Purity was too low to be detected by SDS-PAGE under non-reducing conditions. After receipt, protein was further concentrated using Amicon Ultra-0.5 mL centrifugal filters (Millipore Sigma) prior to use. Proteins were brought up in the same concentration and used for subsequent western analysis under reducing and nonreducing conditions.

Statistics

Data are presented as mean +/- SEM unless otherwise indicated. Statistical tests were performed as appropriate (and noted in the text) using GraphPad Prism software. Statistical significance was defined as $p<0.05$.

Results

Derangements in ER calcium release dynamics in ArcKR neurons

In our previous studies, CA1 field recordings from acute hippocampal slices showed that ArcKR neurons displayed enhanced mGluR-LTD in response to application of S-3,5-dihydroxyphenylglycine (DHPG), including a reduced threshold for reaching LTD and a higher magnitude of LTD (Wall et al., 2018). Because mGluR-LTD is a G_q dependent process requiring release of intracellular Ca^{2+} stores from the ER via ER membrane-bound IP_3Rs, we first explored the possibility that DHPG elicits altered ER Ca^{2+} release in ArcKR neurons.

WT and ArcKR (KR) primary hippocampal neuron cultures were transfected with the ER-localized genetically-encoded calcium indicator G-CatchER$^+$ (Reddish et al., 2021) and imaged on a highly inclined laminated optical sheet (HILO) microscope during the addition of 100 μM S-3,5-DHPG. As the subcellular distribution of Ca^{2+} signaling-related proteins, ER complexity, intracellular [Ca^{2+}], and ER Ca^{2+} release can vary throughout the neuron (Sharp et al., 1993; Terasaki et al., 1994; Spacek and Harris, 1997; Blaustein and Golovina, 2001; Cui-Wang et al., 2012; Krijnse-Locker et al., 2017), we examined various neuronal subregions separately: primary branchpoints (PBs), primary dendrites (PDs), secondary branchpoints (SBs), and secondary dendrites (SDs) (Deng et al., 2021; Reddish et al., 2021) (Figures 1A-1C).

G-CatchER$^+$ fluorescence traces showed a striking depletion of ER Ca^{2+} stores in KR neurons after DHPG application (Figure 1). ER Ca^{2+} release as quantified by percent decrease from baseline average was significantly enhanced in KR neurons at the soma (Figures 1D,E; two-way ANOVA, Genotype: $F(1, 32) = 20.74$, $p < 0.0001$, Time: $F(1, 32) = 10.63$, $p = 0.0026$, Interaction: $F(1, 32) = 18.49$, $p = 0.0001$; Sidak's post-hoc test, WT vs KR at End $p < 0.0001$), PB (Fig. 5F,G; two-way ANOVA, Genotype: $F(1, 32) = 9.120$, $p = 0.0049$, Time: $F(1, 32) = 39.59$, $p < 0.0001$, Interaction: $F(1, 32) = 6.651$, $p = 0.0147$; Sidak's post-hoc test, WT vs KR at End $p = 0.0008$), PD (Figures 1H,I; two-way ANOVA, Genotype: $F(1, 32) = 7.966$, $p = 0.0081$, Time: $F(1, 32) = 24.04$, $p < 0.0001$, Interaction: $F(1, 32) = 7.966$, $p = 0.0063$; Sidak's post-hoc test, WT vs KR at End $p = 0.0006$), and SD (Figures 5L,M; two-way ANOVA, Genotype: $F(1, 32) = 32.51$, $p < 0.0001$, Time: $F(1, 32) = 36.77$, $p < 0.0001$, Interaction: $F(1, 32) = 48.36$, $p < 0.0001$; Sidak's post-hoc test, WT vs KR at End $p < 0.0001$) of KR neurons. However, KR SB showed no difference in release compared to WT neurons (Figures 1J,K; two-way ANOVA, Genotype: $F(1, 32) = 0.3066$, $p = 0.5836$, Time: $F(1, 32) = 8.865$, $p = 0.0055$, Interaction: $F(1, 32) = 0.6407$, $p = 0.4294$), which related to our previous findings that Ca^{2+} release at secondary branchpoints is reduced (Deng et al., 2021; Reddish et al., 2021).

To evaluate if the enhanced Ca^{2+} release in KR neurons was simply due to baseline increases in ER Ca^{2+}, we measured baseline $[Ca^{2+}]_{ER}$ during the application of the ionophore ionomycin (50 μM) in a buffer containing excess Ca^{2+} (10 mM) to saturate the G-CatchER^{+} signal and $[Ca^{2+}]$ was calculated as previously described (de Juan-Sanz et al., 2017) (Figure 2). However, we found no genotype differences in ER Ca^{2+} in any neuronal region examined (Figure 2F; two-way ANOVA, Genotype: $F(1, 41) = 1.133$, $p = 0.2935$, Region: $F(4, 41) = 7.998$, $p < 0.0001$, Interaction: $F(4, 41) = 0.2939$, $p = 0.8803$), indicating that the phenotypes observed in KR neurons were not influenced by baseline $[Ca^{2+}]_{ER}$ prior to DHPG application.

ArcKR displays altered interaction with CaMKII that depends on CaMKII isoform- and phosphorylation status

Previous work has shown that Arc interacts directly with CaMKII, and that this interaction depends on the isoform and phosphorylation status of CaMKII (Okuno et al., 2012; Zhang et al., 2015, 2019). We transfected HEK293 cells with either myc-ArcWT or myc-ArcKR along with GFP-CaMKIIa or GFP-CaMKIIb. We also used CaMKII plasmids with point mutations at Thr286 (for CaMKIIa) or Thr287 (CaMKIIb) that mimic the active, autophosphorylated state (T286D/T287D) or mimic the inactive unphosphorylated state (T286A/T287A) (Bayer et al., 2006a; O'Leary et al., 2006; Coultrap et al., 2012). After immunoprecipitation (IP) of Arc, protein complexes were eluted and immunoblotting proceeded for myc- and GFP-tagged proteins (Figures 3A,C,E,G,I).

While CaMKIIa-GFP interaction with ArcKR was not statistically different from WT (Figure 3B; unpaired t-test with Welch's correction, $t = 0.0607$, $df = 4.289$, $p = 0.9543$), ArcKR interaction was significantly higher with CaMKIIaT286D (Figure 3D; unpaired t-test with Welch's correction, $t = 2.957$, $df = 7.210$, $p = 0.0205$). No difference was detected with CaMKIIaT286A (Figure 3F; unpaired t-test, $t = 0.8050$, $df = 14$, $p = 0.4343$). Interestingly, ArcKR interaction with CamKIIb was significantly higher than WT for both WT CaMKIIb as well as CaMKIIbT287D (Figures 3H,J; CaMKIIb unpaired t-test

with Welch's correction, t = 3.564, df = 7.273, p = 0.0086, CaMKIIbT287D unpaired t-test, t = 2.454, df = 6, p = 0.0495). These results indicate that ArcKR interacts more with CaMKIIb, and that autophosphorylation status of CaMKIIa and CaMKIIb could determine ArcKR interaction.

ArcKR protein exhibits increased self-association

Arc oligomerization has been described to be regulated by Ser-260 phosphorylation by CaMKII (Zhang et al., 2019). Because the mutated lysines of ArcKR (K268/269) are in close proximity to Ser-260 (Mabb et al., 2014; Wall et al., 2018), we sought to determine whether Arc oligomerization potential is altered. We co-transfected HEK293 cells with N-terminal myc-tagged Arc (myc-ArcWT) or ArcKR (myc-ArcKR) and N-terminal GFP-tagged Arc (GFP-Arc) and GFP-ArcKR and performed a co-immunoprecipitation assay to compare the amount of self-association. Immunoblotting following immunoprecipitation of myc-Arc and myc-ArcKR showed that ArcKR self-associates more than WT Arc (Figures 4A,B; unpaired t-test with Welch's correction, t = 3.336, df = 8.199, p = 0.0099). Greater self-pulldown does not indicate oligomerization *per se*, as this method does not differentiate between direct and indirect interactions. Therefore, we next purified WT and ArcKR from HEK 293 cells and performed SDS-PAGE on the purified His-Arc and His-ArcKR proteins under reducing and non-reducing conditions (Figures 4C). Under non-reducing conditions, we observed high molecular weight reactive Arc species in ArcWT and ArcKR. However, there was a prominent band between 100 and 150 kDa in WT but not KR indicating that a fraction of the ArcWT can exist as a dimer (blue asterisk). Under reducing conditions, both WT and KR collapsed into their monomeric forms with prominent bands between 50 and 75 kDa (white asterisk). We thus inferred that ArcKR is more predisposed to forming higher molecular weight oligomers compared to ArcWT.

ArcKR neurons display regional alterations in Arc-CaMKII colocalization

Arc and CaMKII localization and colocalization within subregions of the neuron are critical for several signaling pathways important for learning and memory (Davies et al., 2007; Marsden et al., 2010), including localizing Arc to inactive synapses (Okuno et al., 2012). To discern potential changes in CaMKII localization and colocalization with Arc, we immunostained WT and KR primary hippocampal neuron cultures for CaMKII and Arc and imaged their distributions using confocal microscopy (Figures 5-6).

Two-way ANOVA found no significant genotype difference in Arc protein levels (Figure 5A; two-way ANOVA, Genotype: $F(1, 76) = 1.535$, $p = 0.2192$, Region: $F(3, 76) = 2.890$, $p = 0.0409$, Interaction: $F(3, 76) = 0.2099$, $p = 0.8892$); however, there was a significant effect of region, with secondary branchpoints displaying lower levels than primary dendrites (Tukey's post-hoc test, PD vs SB: $p = 0.0270$). Similarly, CaMKII levels were lower in the secondary branchpoints compared to primary dendrites (Figure 5B; two-way ANOVA, Genotype: $F(1, 76) = 0.3949$, $p = 0.7570$, Region: $F(3, 76) = 3.160$, $p = 0.0294$, Interaction: $F(3, 76) = 0.1961$, $p = 0.6592$, Tukey's post-hoc test PD vs SB: $p = 0.0187$).

We next quantified the colocalization of Arc with total CaMKII from the same samples used in Figures 5. Pixel-pixel Pearson correlation values were lower in KR neurons compared to WT in PBs and PDs but not SBs or SDs (Figure 6A-B; two-way ANOVA, Genotype: $F(1, 111) = 12.54$, $p = 0.0006$, Region: $F(3, 111) = 1.166$, $p = 0.3261$, Interaction: $F(3, 111) = 4.475$, $p = 0.0053$; Sidak's post-hoc test WT vs KR PB $p < 0.0001$, PD $p = 0.0425$, SB $p > 0.9999$, SD $p = 0.9995$). Given the increase in ArcKR interaction with both CamKIIa and CamKIIb constitutive active mutants, we stained WT and KR hippocampal neuron cultures for p-CaMKII and calculated the Arc-p-CaMKII colocalization. However, there were no significant genotype differences (Figure 6C-D; two-way ANOVA Genotype: $F(1, 151) = 0.3609$, $p = 0.5489$, Region: $F (3, 151) = 6.628$, $p = 0.0003$, Interaction: $F (3, 151) = 2.056$, $p = 0.1085$; Sidak's post-hoc test, PB vs PD $p = 0.0003$, PB vs SD $p = 0.0181$).

Because of constraints in resolving isoform-specific changes in CaMKII levels with immunostaining, we used Western blotting to determine if CaMKIIa and CaMKIIb and their respective levels of phosphorylation in WT and KR neuron cultures were altered (Figure 6E). We observed that the proportion of the phosphorylated forms of CaMKIIa (p-CaMKIIa) and CaMKIIb (p-CaMKIIb) were greater in KR neurons (Figure 6F-G; p-CaMKIIa unpaired t-test, $t = 3.015$, $df = 15$, $p = 0.0087$; p-CaMKIIb unpaired t-test, $t = 2.821$, $df = 15$, $p = 0.0129$) but there was no significant difference in the total expression of either isoform (Figures 6H-I; CaMKIIa unpaired t-test, $t = 0.8324$, $df = 15$, $p = 0.4183$; CaMKIIb unpaired t-test, $t = 1.712$, $df = 15$, $p = 0.1075$). Taken together, these results suggest that while ArcKR protein and total CaMKII levels are unchanged in KR neurons, ArcKR is biased toward interacting with p-CaMKII that may occur in a region-dependent manner.

ArcKR has greater interaction with the ER-bound protein calnexin

As we are not aware of any literature implicating Arc levels or posttranslational modifications in regulating ER-mediated Ca^{2+} release, we performed co-immunoprecipitation assays with proteins known to be important for CaMKII or ER function. First, we considered the calcium-sensitive protein calmodulin which is required for CaMKII autophosphorylation (Lisman et al., 2002). However, we were unable to detect an interaction of GFP-tagged calmodulin with ArcWT or ArcKR (Figure 7A).

Arc has also been shown to directly interact with the cytoplasmic tail of the ER membrane-bound protein calnexin, although the functional consequence of this interaction is unknown (Myrum et al., 2017). Intriguingly, calnexin regulates the activity of the sarco/endoplasmic reticulum Ca^{2+}-ATPase (SERCA), another ER-bound protein that sequesters Ca^{2+} in the lumen of the ER (Britzolaki et al., 2020). SERCA2A did not co-immunoprecipitate with either ArcWT or ArcKR (Figure 7B). However, co-immunoprecipitation in HEK293 cells reaffirmed interaction of Arc with calnexin and, notably, revealed that ArcKR protein has an enhanced interaction with Calnexin compared to ArcWT (Figure 7C-D).

Discussion

Previous work has established that disrupting the temporal dynamics of Arc by reducing ubiquitination leads to increased AMPA receptor endocytosis, enhanced mGluR-LTD, and impairments of spatial reversal learning (Wall et al., 2018); however, the intracellular mechanisms by which these phenotypes occurred were unknown. Here we found that disrupting Arc ubiquitination leads to altered ER Ca^{2+} release dynamics in all regions of the neuron with the exception of secondary branchpoints. This phenotype was correlated with increased Arc-CaMKII interactions and Arc self-association. We also demonstrated that Arc ubiquitination and/or turnover may regulate its association with calnexin, providing a possible link between Arc ubiquitination levels and ER functionality.

As mGluR levels remained the same relative to WT, we hypothesized that dysregulation downstream of mGluR activation, such as ER Ca^2 release, may be disrupted in KR neurons. Indeed, we observed that KR neurons release excess ER Ca^{2+} in response to DHPG. While Arc has previously been shown to interact with the cytoplasmic domain of the ER-associated protein calnexin via its central linker region (Myrum et al., 2017), to our knowledge there has never been a study directly implicating Arc in the modulation of ER Ca^2 release dynamics. Interestingly, our co-immunoprecipitation data suggest an increased association of ArcKR with calnexin. How this leads to excess ER Ca^2 release, or more broadly the manner by which Arc impacts ER Ca^2 release, is still unknown and an area of active exploration. It is notable that the activity of SERCA, which is responsible for ER Ca^{2+} refilling (Berridge et al., 2003; Vandecaetsbeek et al., 2009), is modulated by and directly interacts with calnexin (Roderick et al., 2000; Lynes et al., 2013; Gutiérrez et al., 2020). Although we did not observe an interaction of Arc and ArcKR with SERCA, it is possible that a deficiency in Arc ubiquitination may indirectly reduce SERCA activity, perhaps via disrupting interactions between calnexin and SERCA itself. Arc could serve as a “hub” between these proteins, and (as we did not observe any differences in basal [Ca^{2+}]) Arc ubiquitination could act as a mechanistic switch for ensuring rapid ER Ca^{2+} re-sequestration following mGluR activation.

We observed that ArcKR has enhanced interactions with phosphomimetic forms of CaMKIIa and CaMKIIb. CaMKII is important for mGluR-LTD magnitude (Mockett et al., 2011) and its interaction with Arc has previously been established (Okuno et al., 2012; Zhang et al., 2019). Mutations in the CaMKIIa T286 autophosphorylation site were found to block DHPG-induced LTD in hippocampal slices (Zhang et al., 2019). Remarkably, ArcKR neurons exhibit increased GluA2 surface trafficking (Wall et al., 2018), and activated CaMKII has been shown to work in complex with another calcium-regulated protein PICK1 (protein interacting with C-kinase 1) to facilitate GluA2 trafficking from the ER to the cell surface in an ER Ca^{2+} release-dependent manner (Lu et al., 2014). Notably, GluA2 undergoes Q/R editing, decreasing AMPA receptor Ca^{2+} permeability (Bowie and Mayer, 1995; Plant et al., 2006; Zhou et al., 2017), hinting at a potential compensatory effect of elevated calcium signaling in ArcKR neurons. Arc itself is known to interact with PICK1 via the PICK1 BAR domain, with the interaction and spatial distribution of the two proteins altered under depolarizing conditions (Goo et al., 2018). While we did not probe PICK1 in any of our experiments, we did observe that the colocalization of Arc with total CaMKII was decreased at PBs and PDs. When coupled with the lack of any differences in colocalization with p-CaMKII, this hints at a possible link between the increased preference of ArcKR to interact with p-CaMKII and Arc-PICK1 interaction that leads to altered AMPA receptor trafficking dynamics.

We found that ArcKR has increased self-association compared to ArcWT. Using SDS-PAGE under non-reducing conditions, we observed signs that ArcKR may be biased for increased oligomerization. Interestingly, Arc oligomerization is negatively regulated via phosphorylation at Ser 260 by CaMKII. Mutation of CaMKII phosphorylation sites on Arc leads to enhanced mGluR-LTD and causes impairments in the acquisition of fear induced memories (Zhang et al., 2019). Mirroring that work, we also found that ArcKR mice have impaired fear memories (data not shown). Given these correlates, one possibility is that the ArcKR mutation reduces CamKII-dependent phosphorylation at Ser 260. Conversely, it is unknown if Arc CamKII-dependent phosphorylation sites regulate its ubiquitination which may alter ER-mediated Ca^{2+} release.

Given the literature and our findings, we propose a mechanism whereby CaMKII-dependent phosphorylation of Arc promotes Arc ubiquitination, which in turn tempers ER-mediated Ca^{2+} release to promote synaptic strengthening via reducing AMPA receptor endocytosis. In this model, CaMKII auto-phosphorylation marks a synapse for strengthening, and p-CaMKII interacts preferentially with non-ubiquitinated Arc. CamKII then phosphorylates Arc at Ser 260, increasing its ubiquitination. This serves to counteract Arc activity by 1) attenuating type 1 mGluR-activation-mediated ER Ca^{2+} release, 2) promoting Arc degradation via the ubiquitin-proteasome pathway, and 3) subsequently tempering AMPA receptor endocytosis. This mechanism would explain the increased ArcKR interaction with CaMKII. An additional consideration is that Arc ubiquitination also regulates Ser 260 phosphorylation. Given our observed spatial differences in Arc localization in neurons and correlations to ER-mediated Ca^{2+} release, this mechanism could be a way in which neurons provide regional specificity along dendritic regions to fine-tune synaptic strength in response to select synaptic inputs.

Arc-dependent intracellular Ca^{2+} dysregulation carries important implications for behavioral output. ArcKR mice exhibit impaired spatial reversal learning on a Barnes maze task which was associated with enhanced mGluR-LTD (Wall et al., 2018). Further work is aimed at determining whether this behavioral deficit is also due in part to other ArcKR effects observed in this study. For example, dysregulation of CaMKII phosphorylation has been shown to affect strategy selection on the Barnes maze (Bach et al., 1995). Furthermore, n-methyl-d-aspartate receptor-mediated LTD is required for behavioral flexibility on a similarly spatial learning-dependent Morris water maze task (Nicholls et al., 2008; Kim et al., 2011). Prevention of LTD induction and reduction of AMPA receptor endocytosis caused by stabilization of the adhesion molecule β-catenin causes similar deficits in reversal learning on the water maze (Mills et al., 2014). Enhanced Arc translation is found to occur in Fragile X-syndrome model mice, which also display enhanced mGluR-LTD and increased AMPA receptor endocytosis (Hou et al., 2006; Nakamoto et al., 2007; Cheng et al., 2017). It is possible that this model has increased DHPG-induced ER-Ca^{2+} release similar to our ArcKR mice. Tempering ER-

Ca^{2+} release via increases in Arc ubiquitination might serve as an alternative mechanism that could restore excessive mGluR-LTD in this mouse model. Cumulatively, our ArcKR model suggests that the cooperation of different forms of LTD within an optimal magnitude, threshold, and temporal range are necessary for optimal behavioral outputs – whether some of these are regulated by Arc ubiquitination, Arc-CaMKII interaction, and regulation of ER Ca^{2+} release is a subject for future research.

Conflict of Interest

J.J.Y. is the shareholder of InLighta Biosciences and is a named inventor on an issued patent (US10371708). All other authors declare no conflicts of interest.

Author Contributions

MAG designed the study, performed experiments, and wrote the manuscript. ZDA, CLM, and BD performed experiments. NF and JJY contributed to study design. AMM designed the study, edited the manuscript, and contributed to manuscript writing.

Funding

This study was funded by the Whitehall Foundation (Grant 2017-05-35), NSF Career Award (2047700), and NARSAD Young Investigator Grant from the Brain & Behavior Research Foundation Research Partners Program (P&S Fund Investigator, 28549) to AMM; NIGMS (Grant R01GM115763) and Georgia State University startup funds to N.F. Georgia State University Second Century Initiative Neurogenomics Fellowship, Georgia State University Brains & Behavior Fellowship, and Kenneth W. and Georganne F. Honeycutt Fellowship to MAG.

Acknowledgements

We would like to thank Dr. Ulli Bayer for providing the CaMKII constructs, the Neuroscience Institute confocal core staff, and GSU Division of Animal Resources for providing excellent animal care.

References

Abe, T., Sugihara, H., Nawa, H., Shigemoto, R., Mizuno, N., and Nakanishi, S. (1992). Molecular characterization of a novel metabotropic glutamate receptor mGluR5 coupled to inositol phosphate/Ca2+ signal transduction. *Journal of Biological Chemistry* 267, 13361–13368. doi: 10.1016/S0021-9258(18)42219-3.

Aramori, I., and Nakanishi, S. (1992). Signal transduction and pharmacological characteristics of a metabotropic glutamate receptor, mGluRI, in transfected CHO cells. *Neuron* 8, 757–765. doi: 10.1016/0896-6273(92)90096-V.

Bach, M. E., Hawkins, R. D., Osman, M., Kandel, E. R., and Mayford, M. (1995). Impairment of spatial but not contextual memory in CaMKII mutant mice with a selective loss of hippocampal LTP in the range of the theta frequency. *Cell* 81, 905–915. doi: 10.1016/0092-8674(95)90010-1.

Bayer, K. U., LeBel, É., McDonald, G. L., O'Leary, H., Schulman, H., and de Koninck, P. (2006a). Transition from Reversible to Persistent Binding of CaMKII to Postsynaptic Sites and NR2B. *Journal of Neuroscience* 26, 1164–1174. doi: 10.1523/JNEUROSCI.3116-05.2006.

Bayer, K. U., Ric Lebel, E. ´, Mcdonald, G. L., O'leary, H., Schulman, H., and de Koninck, P. (2006b). Transition from Reversible to Persistent Binding of CaMKII to Postsynaptic Sites and NR2B. doi: 10.1523/JNEUROSCI.3116-05.2006.

Bayer, K. U., and Schulman, H. (2019). CaM Kinase: Still Inspiring at 40. *Neuron* 103, 380–394. doi: 10.1016/J.NEURON.2019.05.033.

Beique, J. C., Na, Y., Kuhl, D., Worley, P. F., and Huganir, R. L. (2011). Arc-dependent synapse-specific homeostatic plasticity. *Proc Natl Acad Sci U S A* 108, 816–821. doi: 10.1073/pnas.1017914108.

Berridge, M. J., Bootman, M. D., and Roderick, H. L. (2003). Calcium signalling: dynamics, homeostasis and remodelling. *Nature Reviews Molecular Cell Biology 2003 4:7* 4, 517–529. doi: 10.1038/nrm1155.

Blaustein, M. P., and Golovina, V. A. (2001). Structural complexity and functional diversity of endoplasmic reticulum Ca2+ stores. *Trends Neurosci* 24, 602–608. doi: 10.1016/S0166-2236(00)01891-9.

Bowie, D., and Mayer, M. L. (1995). Inward rectification of both AMPA and kainate subtype glutamate receptors generated by polyamine-mediated ion channel block. *Neuron* 15, 453–462. doi: 10.1016/0896-6273(95)90049-7.

Bramham, C. R., Worley, P. F., Moore, M. J., and Guzowski, J. F. (2008). The immediate early gene arc/arg3.1: regulation, mechanisms, and function. *J Neurosci* 28, 11760–11767. doi: 10.1523/JNEUROSCI.3864-08.2008.

Britzolaki, A., Saurine, J., Klocke, B., and Pitychoutis, P. M. (2020). A Role for SERCA Pumps in the Neurobiology of Neuropsychiatric and Neurodegenerative Disorders. *Adv Exp Med Biol* 1131, 131–161. doi: 10.1007/978-3-030-12457-1_6/COVER.

Cheng, G.-R., Xiang, Y.-D., Liu, D., Mcclintock, S. M., Zeng, Y., and Zeng, Y. (2017). The Implication of AMPA Receptor in Synaptic Plasticity Impairment and Intellectual Disability in Fragile X Syndrome. *Physiol. Res* 66, 715–727. Available at: www.biomed.cas.cz/physiolres [Accessed August 21, 2022].

Chowdhury, S., Shepherd, J. D., Okuno, H., Lyford, G., Petralia, R. S., Plath, N., et al. (2006). Arc/Arg3.1 interacts with the endocytic machinery to regulate AMPA receptor trafficking. *Neuron* 52, 445–459. doi: S0896-6273(06)00682-9 [pii] 10.1016/j.neuron.2006.08.033.

Cook, S. G., Rumian, N. L., and Bayer, K. U. (2022). CaMKII T286 phosphorylation has distinct essential functions in three forms of long-term plasticity. *Journal of Biological Chemistry* 298, 102299. doi: 10.1016/J.JBC.2022.102299.

Coultrap, S. J., Barcomb, K., and Bayer, K. U. (2012). A Significant but Rather Mild Contribution of T286 Autophosphorylation to Ca2+/CaM-Stimulated CaMKII Activity. *PLoS One* 7, e37176. doi: 10.1371/JOURNAL.PONE.0037176.

Coultrap, S. J., Freund, R. K., O'Leary, H., Sanderson, J. L., Roche, K. W., Dell'Acqua, M. L., et al. (2014). Autonomous CaMKII Mediates Both LTP and LTD Using a

Mechanism for Differential Substrate Site Selection. *Cell Rep* 6, 431–437. doi: 10.1016/J.CELREP.2014.01.005.

Cui-Wang, T., Hanus, C., Cui, T., Helton, T., Bourne, J., Watson, D., et al. (2012). Local Zones of Endoplasmic Reticulum Complexity Confine Cargo in Neuronal Dendrites. *Cell* 148, 309–321. doi: 10.1016/J.CELL.2011.11.056.

Davies, K. D., Alvestad, R. M., Coultrap, S. J., and Browning, M. D. (2007). αCaMKII autophosphorylation levels differ depending on subcellular localization. *Brain Res* 1158, 39–49. doi: 10.1016/J.BRAINRES.2007.05.008.

de Juan-Sanz, J., Holt, G. T., Schreiter, E. R., de Juan, F., Kim, D. S., and Ryan, T. A. (2017). Axonal Endoplasmic Reticulum Ca2+ Content Controls Release Probability in CNS Nerve Terminals. *Neuron* 93. doi: 10.1016/j.neuron.2017.01.010.

Deng, X., Yao, X. I.-Q., Kenberglund, B., Dong, D., Ouedraogo, M. A., Ghane, Y., et al. (2021). Tuning Protein Dynamics to Sense Rapid Endoplasmic-Reticulum Calcium Dynamics. *Angewandte Chemie* 133, 23477–23486. doi: 10.1002/ANGE.202108443.

Donai, H., Sugiura, H., Ara, D., Yoshimura, Y., Yamagata, K., and Yamauchi, T. (2003). Interaction of Arc with CaM kinase II and stimulation of neurite extension by Arc in neuroblastoma cells expressing CaM kinase II. *Neurosci Res* 47, 399–408. doi: 10.1016/J.NEURES.2003.08.004.

Elgersma, Y., Fedorov, N. B., Ikonen, S., Choi, E. S., Elgersma, M., Carvalho, O. M., et al. (2002). Inhibitory Autophosphorylation of CaMKII Controls PSD Association, Plasticity, and Learning. *Neuron* 36, 493–505. doi: 10.1016/S0896-6273(02)01007-3.

Gillespie, J. M., and Hodge, J. J. L. (2013). CASK regulates CaMKII autophosphorylation in neuronal growth, calcium signaling, and learning. *Front Mol Neurosci* 6, 27. doi: 10.3389/FNMOL.2013.00027/BIBTEX.

Glazewski, S., Giese, K. P., Silva, A., and Fox, K. (2000). The role of α-CaMKII autophosphorylation in neocortical experience-dependent plasticity. *Nature Neuroscience 2000 3:9* 3, 911–918. doi: 10.1038/78820.

Goo, B. M. S. S., Sanstrum, B. J., Holden, D. Z. Y., Yu, Y., and James, N. G. (2018). Arc/Arg3.1 has an activity-regulated interaction with PICK1 that results in altered

spatial dynamics. *Scientific Reports 2018 8:1* 8, 1–12. doi: 10.1038/s41598-018-32821-4.

Gutiérrez, T., Qi, H., Yap, M. C., Tahbaz, N., Milburn, L. A., Lucchinetti, E., et al. (2020). The ER chaperone calnexin controls mitochondrial positioning and respiration. *Sci Signal* 13. doi: 10.1126/SCISIGNAL.AAX6660.

Guzowski, J. F., McNaughton, B. L., Barnes, C. A., and Worley, P. F. (1999). Environment-specific expression of the immediate-early gene Arc in hippocampal neuronal ensembles. *Nat Neurosci* 2, 1120–1124. doi: 10.1038/16046.

Hou, L., Antion, M. D., Hu, D., Spencer, C. M., Paylor, R., and Klann, E. (2006). Dynamic Translational and Proteasomal Regulation of Fragile X Mental Retardation Protein Controls mGluR-Dependent Long-Term Depression. *Neuron* 51, 441–454. doi: 10.1016/J.NEURON.2006.07.005.

Husain, N., Yuan, Q., Yen, Y. C., Pletnikova, O., Sally, D. Q., Worley, P., et al. (2017). TRIAD3/RNF216 mutations associated with Gordon Holmes syndrome lead to synaptic and cognitive impairments via Arc misregulation. *Aging Cell* 16, 281–292. doi: 10.1111/acel.12551.

Jenks, K. R., Kim, T., Pastuzyn, E. D., Okuno, H., Taibi, A. v, Bito, H., et al. (2017). Arc restores juvenile plasticity in adult mouse visual cortex. *Proc Natl Acad Sci U S A*. doi: 10.1073/pnas.1700866114.

Kim, J. I., Lee, H. R., Sim, S. E., Baek, J., Yu, N. K., Choi, J. H., et al. (2011). PI3Kγ is required for NMDA receptor–dependent long-term depression and behavioral flexibility. *Nature Neuroscience 2011 14:11* 14, 1447–1454. doi: 10.1038/nn.2937.

Korb, E., and Finkbeiner, S. (2011). Arc in synaptic plasticity: from gene to behavior. *Trends Neurosci* 34, 591–598. doi: 10.1016/j.tins.2011.08.007.

Krijnse-Locker, J., Parton, R. G., Fuller, S. D., Griffiths, G., and Dotti, C. G. (2017). The organization of the endoplasmic reticulum and the intermediate compartment in cultured rat hippocampal neurons. *https://doi.org/10.1091/mbc.6.10.1315* 6, 1315–1332. doi: 10.1091/MBC.6.10.1315.

Lisman, J., Schulman, H., and Cline, H. (2002). The molecular basis of CaMKII function in synaptic and behavioural memory. *Nature Reviews Neuroscience 2002 3:3* 3, 175–190. doi: 10.1038/nrn753.

Lu, W., Khatri, L., and Ziff, E. B. (2014). Trafficking of α-Amino-3-hydroxy-5-methyl-4-isoxazolepropionic Acid Receptor (AMPA) Receptor Subunit GluA2 from the Endoplasmic Reticulum Is Stimulated by a Complex Containing Ca2+/Calmodulin-activated Kinase II (CaMKII) and PICK1 Protein and by Release of Ca2+ from Internal Stores *. *Journal of Biological Chemistry* 289, 19218–19230. doi: 10.1074/JBC.M113.511246.

Lyford, G. L., Yamagata, K., Kaufmann, W. E., Barnes, C. A., Sanders, L. K., Copeland, N. G., et al. (1995). Arc, a growth factor and activity-regulated gene, encodes a novel cytoskeleton-associated protein that is enriched in neuronal dendrites. *Neuron* 14, 433–445. doi: 0896-6273(95)90299-6 [pii].

Lynes, E. M., Raturi, A., Shenkman, M., Sandoval, C. O., Yap, M. C., Wu, J., et al. (2013). Palmitoylation is the switch that assigns calnexin to quality control or ER Ca2+ signaling. *J Cell Sci* 126, 3893–3903. doi: 10.1242/JCS.125856/263469/AM/PALMITOYLATION-IS-THE-SWITCH-THAT-ASSIGNS-CALNEXIN.

Mabb, A. M., and Ehlers, M. D. (2018). Arc ubiquitination in synaptic plasticity. *Semin Cell Dev Biol* 77, 10–16. doi: 10.1016/j.semcdb.2017.09.009.

Mabb, A. M., Je, H. S., Wall, M. J., Robinson, C. G., Larsen, R. S., Qiang, Y., et al. (2014). Triad3A regulates synaptic strength by ubiquitination of Arc. *Neuron* 82, 1299–1316. doi: 10.1016/j.neuron.2014.05.016.

Marsden, K. C., Shemesh, A., Bayer, K. U., and Carroll, R. C. (2010). Selective translocation of Ca2+/calmodulin protein kinase IIα (CaMKIIα) to inhibitory synapses. *Proc Natl Acad Sci U S A* 107, 20559–20564. doi: 10.1073/PNAS.1010346107/-/DCSUPPLEMENTAL.

Mills, F., Bartlett, T. E., Dissing-Olesen, L., Wisniewska, M. B., Kuznicki, J., Macvicar, B. A., et al. (2014). Cognitive flexibility and long-term depression (LTD) are impaired following β-catenin stabilization in vivo. *Proc Natl Acad Sci U S A* 111, 8631–8636. doi: 10.1073/PNAS.1404670111/SUPPL_FILE/PNAS.1404670111.SM01.AVI.

Mockett, B. G., Guévremont, D., Wutte, M., Hulme, S. R., Williams, J. M., and Abraham, W. C. (2011). Calcium/Calmodulin-Dependent Protein Kinase II Mediates Group I Metabotropic Glutamate Receptor-Dependent Protein Synthesis and Long-Term

Depression in Rat Hippocampus. *Journal of Neuroscience* 31, 7380–7391. doi: 10.1523/JNEUROSCI.6656-10.2011.

Moga, D. E., Calhoun, M. E., Chowdhury, A., Worley, P., Morrison, J. H., and Shapiro, M. L. (2004). Activity-regulated cytoskeletal-associated protein is localized to recently activated excitatory synapses. *Neuroscience* 125, 7–11. doi: 10.1016/J.NEUROSCIENCE.2004.02.004.

Murakoshi, H., Shin, M. E., Parra-Bueno, P., Szatmari, E. M., Shibata, A. C. E., and Yasuda, R. (2017). Kinetics of Endogenous CaMKII Required for Synaptic Plasticity Revealed by Optogenetic Kinase Inhibitor. *Neuron* 94, 37-47.e5. doi: 10.1016/J.NEURON.2017.02.036.

Myrum, C., Soulé, J., Bittins, M., Cavagnini, K., Goff, K., Ziemek, S. K., et al. (2017). Arc interacts with the integral endoplasmic reticulum protein, calnexin. *Front Cell Neurosci* 11, 294. doi: 10.3389/FNCEL.2017.00294/BIBTEX.

Nakamoto, M., Nalavadi, V., Epstein, M. P., Narayanan, U., Bassell, G. J., and Warren, S. T. (2007). Fragile X mental retardation protein deficiency leads to excessive mGluR5-dependent internalization of AMPA receptors. *Proc Natl Acad Sci U S A* 104, 15537–15542. doi: 10.1073/PNAS.0707484104/SUPPL_FILE/07484FIG7.PDF.

Nakayama, D., Iwata, H., Teshirogi, C., Ikegaya, Y., Matsuki, N., and Nomura, H. (2015). Long-delayed expression of the immediate early gene Arc/Arg3.1 refines neuronal circuits to perpetuate fear memory. *J Neurosci* 35, 819–830. doi: 10.1523/JNEUROSCI.2525-14.2015.

Newpher, T. M., Harris, S., Pringle, J., Hamilton, C., and Soderling, S. (2018). Regulation of spine structural plasticity by Arc/Arg3.1. *Semin Cell Dev Biol* 77, 25–32. doi: 10.1016/j.semcdb.2017.09.022.

Nicholls, R. E., Alarcon, J. M., Malleret, G., Carroll, R. C., Grody, M., Vronskaya, S., et al. (2008). Transgenic Mice Lacking NMDAR-Dependent LTD Exhibit Deficits in Behavioral Flexibility. *Neuron* 58, 104–117. doi: 10.1016/J.NEURON.2008.01.039.

Okuno, H., Akashi, K., Ishii, Y., Yagishita-Kyo, N., Suzuki, K., Nonaka, M., et al. (2012). Inverse synaptic tagging of inactive synapses via dynamic interaction of Arc/Arg3.1 with CaMKIIbeta. *Cell* 149, 886–898. doi: 10.1016/j.cell.2012.02.062.

O'Leary, H., Lasda, E., and Bayer, K. U. (2006). CaMKIIβ association with the actin cytoskeleton is regulated by alternative splicing. *Mol Biol Cell* 17, 4656–4665. doi: 10.1091/MBC.E06-03-0252/ASSET/IMAGES/LARGE/ZMK0110678360007.JPEG.

Palmer, M. J., Irving, A. J., Seabrook, G. R., Jane, D. E., and Collingridge, G. L. (1997). The group I mGlu receptor agonist DHPG induces a novel form of LTD in the CA1 region of the hippocampus. *Neuropharmacology* 36, 1517–1532. doi: 10.1016/S0028-3908(97)00181-0.

Pastuzyn, E. D., and Shepherd, J. D. (2017). Activity-Dependent Arc Expression and Homeostatic Synaptic Plasticity Are Altered in Neurons from a Mouse Model of Angelman Syndrome. *Front Mol Neurosci* 10, 234. doi: 10.3389/fnmol.2017.00234.

Peebles, C. L., Yoo, J., Thwin, M. T., Palop, J. J., Noebels, J. L., and Finkbeiner, S. (2010). Arc regulates spine morphology and maintains network stability in vivo. *Proc Natl Acad Sci U S A* 107, 18173–18178. doi: 10.1073/PNAS.1006546107.

Plant, K., Pelkey, K. A., Bortolotto, Z. A., Morita, D., Terashima, A., Mcbain, C. J., et al. (2006). Transient incorporation of native GluR2-lacking AMPA receptors during hippocampal long-term potentiation. doi: 10.1038/nn1678.

Plath, N., Ohana, O., Dammermann, B., Errington, M. L., Schmitz, D., Gross, C., et al. (2006). Arc/Arg3.1 is essential for the consolidation of synaptic plasticity and memories. *Neuron* 52, 437–444. doi: S0896-6273(06)00646-5 [pii] 10.1016/j.neuron.2006.08.024.

Ramirez-Amaya, V., Vazdarjanova, A., Mikhael, D., Rosi, S., Worley, P. F., and Barnes, C. A. (2005). Spatial exploration-induced Arc mRNA and protein expression: evidence for selective, network-specific reactivation. *J Neurosci* 25, 1761–1768. doi: 10.1523/JNEUROSCI.4342-04.2005.

Rao, V. R., Pintchovski, S. A., Chin, J., Peebles, C. L., Mitra, S., and Finkbeiner, S. (2006). AMPA receptors regulate transcription of the plasticity-related immediate-early gene Arc. *Nat Neurosci* 9, 887–895. doi: nn1708 [pii] 10.1038/nn1708.

Reddish, F. N., Miller, C. L., Deng, X., Dong, B., Patel, A. A., Ghane, M. A., et al. (2021). Rapid subcellular calcium responses and dynamics by calcium sensor G-CatchER+. *iScience* 24, 102129. doi: 10.1016/J.ISCI.2021.102129.

Roderick, H. L., Lechleiter, J. D., and Camacho, P. (2000). Cytosolic Phosphorylation of Calnexin Controls Intracellular Ca2+ Oscillations via an Interaction with Serca2b. *Journal of Cell Biology* 149, 1235–1248. doi: 10.1083/JCB.149.6.1235.

Rossetti, T., Banerjee, S., Kim, C., Leubner, M., Lamar, C., Gupta, P., et al. (2017). Memory Erasure Experiments Indicate a Critical Role of CaMKII in Memory Storage. *Neuron* 96, 207-216.e2. doi: 10.1016/J.NEURON.2017.09.010.

Sharp, A. H., McPherson, P. S., Dawson, T. M., Aoki, C., Campbell, K. P., and Snyder, S. H. (1993). Differential immunohistochemical localization of inositol 1,4,5-trisphosphate- and ryanodine-sensitive Ca2+ release channels in rat brain. *Journal of Neuroscience* 13, 3051–3063. doi: 10.1523/JNEUROSCI.13-07-03051.1993.

Shepherd, J. D., Rumbaugh, G., Wu, J., Chowdhury, S., Plath, N., Kuhl, D., et al. (2006). Arc/Arg3.1 mediates homeostatic synaptic scaling of AMPA receptors. *Neuron* 52, 475–484. doi: S0896-6273(06)00683-0 [pii] 10.1016/j.neuron.2006.08.034.

Snyder, E. M., Philpot, B. D., Huber, K. M., Dong, X., Fallon, J. R., and Bear, M. F. (2001). Internalization of ionotropic glutamate receptors in response to mGluR activation. *Nature Neuroscience 2001 4:11* 4, 1079–1085. doi: 10.1038/nn746.

Spacek, J., and Harris, K. M. (1997). Three-Dimensional Organization of Smooth Endoplasmic Reticulum in Hippocampal CA1 Dendrites and Dendritic Spines of the Immature and Mature Rat. *Journal of Neuroscience* 17, 190–203. doi: 10.1523/JNEUROSCI.17-01-00190.1997.

Steward, O., Wallace, C. S., Lyford, G. L., and Worley, P. F. (1998). Synaptic Activation Causes the mRNA for the IEG Arc to Localize Selectively near Activated Postsynaptic Sites on Dendrites. *Neuron* 21, 741–751. doi: 10.1016/S0896-6273(00)80591-7.

Terasaki, M., Slater, N. T., Fein, A., Schmidek, A., and Reese, T. S. (1994). Continuous network of endoplasmic reticulum in cerebellar Purkinje neurons. *Proc Natl Acad Sci U S A* 91, 7510–7514. doi: 10.1073/PNAS.91.16.7510.

Vandecaetsbeek, I., Trekels, M., de Maeyer, M., Ceulemans, H., Lescrinier, E., Raeymaekers, L., et al. (2009). Structural basis for the high Ca2+ affinity of the

ubiquitous SERCA2b Ca2+ pump. *Proc Natl Acad Sci U S A* 106, 18533–18538. doi: 10.1073/PNAS.0906797106/SUPPL_FILE/0906797106SI.PDF.

Wall, M. J., Collins, D. R., Chery, S. L., Allen, Z. D., Pastuzyn, E. D., George, A. J., et al. (2018). The Temporal Dynamics of Arc Expression Regulate Cognitive Flexibility. *Neuron* 98, 1124-1132 e7. doi: 10.1016/j.neuron.2018.05.012.

Wilkerson, J. R., Albanesi, J. P., and Huber, K. M. (2018). Roles for Arc in metabotropic glutamate receptor-dependent LTD and synapse elimination: Implications in health and disease. *Semin Cell Dev Biol* 77, 51–62. doi: 10.1016/J.SEMCDB.2017.09.035.

Yan, J., Porch, M. W., Court-Vazquez, B., Bennett, M. V. L., and Zukin, R. S. (2018). Activation of autophagy rescues synaptic and cognitive deficits in fragile X mice. *Proc Natl Acad Sci U S A* 115, E9707–E9716. doi: 10.1073/PNAS.1808247115/SUPPL_FILE/PNAS.1808247115.SAPP.PDF.

Zhang, H., and Bramham, C. R. (2020). Arc/Arg3.1 function in long-term synaptic plasticity: Emerging mechanisms and unresolved issues. *Eur J Neurosci*. doi: 10.1111/ejn.14958.

Zhang, W., Chuang, Y. A., Na, Y., Ye, Z., Yang, L., Lin, R., et al. (2019). Arc Oligomerization Is Regulated by CaMKII Phosphorylation of the GAG Domain: An Essential Mechanism for Plasticity and Memory Formation. *Mol Cell* 75. doi: 10.1016/j.molcel.2019.05.004.

Zhang, W., Wu, J., Ward, M. D., Yang, S., Chuang, Y. A., Xiao, M., et al. (2015). Structural basis of arc binding to synaptic proteins: implications for cognitive disease. *Neuron* 86, 490–500. doi: 10.1016/j.neuron.2015.03.030.

Zhou, Z., Liu, A., Xia, S., Leung, C., Qi, J., Meng, Y., et al. (2017). The C-terminal tails of endogenous GluA1 and GluA2 differentially contribute to hippocampal synaptic plasticity and learning. *Nature Neuroscience 2017 21:1* 21, 50–62. doi: 10.1038/s41593-017-0030-z.

Figure Legends

Figure 1. DHPG elicits excess ER Ca^{2+} release with disrupted dynamics in ArcKR hippocampal neurons. **(A)** Schematic of regions of interest referred to in this figure. **(B)** Representative image from a G-CatchER^{+}-transfected ArcWT neuron (**C**) Representative image from a G-CatchER^{+}-transfected ArcKR neuron. **(D, F, H, J, L)** Normalized G-CatchER^{+} signal for WT (blue, N = 6 neurons) and ArcKR (red, N = 12 neurons) primary hippocampal neurons in the region of the neuron indicated with application 100 μM DHPG (black bar). Mean percent change from baseline (0-75 s) +/- SEM. Soma n = 6 WT, 12 KR; primary branchpoint n = 13 WT, 25 KR; primary dendrite n = 6 WT, 12 KR; secondary branchpoint n = 16 WT, 14 KR; secondary dendrites n = 14 WT, 24 KR. **(E, G, I, K, M)** Mean G-CatchER^{+} fluorescence decrease from mean baseline fluorescence (0-75 s) at wash-in of DHPG and at 800 s ArcWT (blue) and ArcKR (red) primary hippocampal neurons. Mean +/- SEM. Two-way ANOVA with Šídák's multiple comparison test; * $p < 0.05$, ** $p < 0.01$, *** $p < 0.001$, **** $p < 0.0001$, ns $p > 0.05$.

Figure 2. Baseline ER [Ca^{2+}] is not different in ArcKR primary hippocampal neurons. **(A-E)** Mean G-CatchER^{+} fluorescence change from baseline (0-75 s) at the indicated regions during application of 50 μM ionomycin + 10 mM Ca^{2+} to ArcWT (blue, N = 3) and ArcKR (red, N = 4) primary hippocampal neurons. Mean +/- SEM. Soma n = 3 WT, 4 KR; primary branchpoint n = 8 WT, 8 KR; primary dendrite n = 8 WT, 8 KR; secondary branchpoint n = 4 WT, 3 KR; secondary dendrites n = 3 WT, 2 KR. **(F)** Calculated $[Ca^{2+}]_{ER}$ for ArcWT and ArcKR neurons. Mean +/- SEM. Two-way ANOVA with Šídák's multiple comparison test, no significant genotype effects. Significant simple effect of region ($F(4, 41)$, $p < 0.0001$).

Figure 3. ArcKR protein differentially interacts with CaMKII in an isoform- and phosphorylation status-dependent manner. **(A, C, E, G, I)** Representative Western blots after pulldown of myc-Arc and immunoblotted for the indicated tags. **(B)** Quantification of GFP-CaMKIIa after IP myc-ArcWT (blue) or myc-ArcKR (red). **(D)** Quantification of GFP-CaMKIIaT286D after IP of myc-ArcWT or myc-ArcKR. Unpaired t-test with Welch's

correction for unequal variances, t = 2.957, df = 7.210, * p = 0.0205. **(E)** Quantification of GFP-CaMKIIaT286A after IP of myc-ArcWT or myc-ArcKR. Unpaired t-test with Welch's correction for unequal variances, t = 0.8050, df = 14, p = 0.4343. **(H)** Quantification of GFP-CaMKIIb after IP of myc-ArcWT or myc-ArcKR. Unpaired t-test with Welch's correction for unequal variances, t = 3.564, df = 7.273, ** p = 0.0086. Mean +/- SEM. **(J)** Quantification of GFP-CaMKIIbT287D after IP of myc-ArcWT or myc-ArcKR. Unpaired t-test, t = 2.454, df = 6, * p = 0.0495.

Figure 4. ArcKR self-association is increased relative to ArcWT. **(A)** Representative Western blots after pulldown of myc-ArcWT or myc-ArcKR with an anti-myc antibody and immunoblotted with anti-GFP to detect GFP-ArcWT or GFP-ArcKR. **(B)** Quantification of GFP-ArcWT or GFP-ArcKR after pulldown with myc-Arc or myc-ArcKR. t-test with Welch's correction for unequal variances, t = 3.336, df = 8.199, ** p = 0.0099. **(C)** His-ArcWT and His-ArcKR under non-reducing (- 2-ME) and reducing conditions (+ 2-ME). *Left*, total protein stain for Arc. *Right*, Immunoblot using an anti-Arc polyclonal antibody (blue * represents predicted Arc dimer, white * represents predicted Arc monomer).

Figure 5. Arc and CaMKII is decreased at secondary branchpoints in ArcWT and ArcKR primary hippocampal neurons. **(A)** Fold change of Arc integrated densities for the indicated regions in ArcWT (blue, N = 7) and ArcKR (red, N = 5) primary hippocampal neurons relative to ArcWT PB. Primary branchpoint n = 12 WT, 11 ArcKR; primary dendrite n = 9 WT, 10 ArcKR; secondary branchpoint n = 10 WT, 11 ArcKR; secondary dendrites n = 10 WR, 11 ArcKR. Tukey's post-hoc test, PD vs SB: *p = 0.0270. **(B)** CaMKII integrated densities for indicated regions in (A). Tukey's post-hoc test PD vs SB: *p = 0.0187. **(C)** Representative confocal images from ArcWT and ArcKR primary hippocampal neurons. Scale bar = 20 µm.

Figure 6. Global and regional alterations in Arc-CaMKII colocalization in ArcKR hippocampal neurons. **(A)** Pearson correlation coefficient between CaMKII and Arc in

ArcWT (blue, N = 7) and ArcKR (red, N = 5) primary hippocampal neurons. Primary branchpoint n = 18 WT, 18 KR; primary dendrite n = 15 WT, 14 KR; secondary branchpoint n = 10 WT, 10 KR; secondary dendrites n = 18 WT, 16 KR. Two-way ANOVA with Šídák's multiple comparison test, effect of genotype ($F(1, 111) = 12.54$, $p < 0.0006$, interaction $F(3,111) = 4.475$, $p = 0.0053$). * $p < 0.05$, **** $p < 0.0001$, ns $p > 0.05$. Mean +/- SEM. **(B)** Representative pixel-pixel correlation heatmap between Arc and CaMKII for an ArcWT and ArcKR neuron (left) and corresponding pixel-pixel intensity plots with trendline (right). Scale bar = 20 µm. **(C)** Pearson correlation coefficient between p-CaMKII and Arc in ArcWT (blue, N = 7) and ArcKR (red, N = 9) primary hippocampal neurons. Primary branchpoint n = 18 WT, 27 KR; primary dendrite n = 17 WT, 28 KR; secondary branchpoint n = 13 WT, 18 KR; secondary dendrites n = 15 WT, 23 KR. Two-way ANOVA with Šídák's multiple comparison test. Mean +/- SEM. **(D)** Representative pixel-pixel correlation heatmap between Arc and p-CaMKII for a WT and KR neuron (left) and corresponding pixel-pixel plots with trendline (right). Scale bar = 20 µm. **(E)** Representative Western blots for (F-I). **(F)** Quantification of Western blot for p-CaMKIIα normalized to total CaMKIIα. Unpaired t-test ($t = 3.015$, $df = 15$, ** $p = 0.0087$). **(G)** Quantification of Western blot for p-CaMKIIβ normalized to total CaMKIIβ. Unpaired t-test ($t = 2.821$, $df = 15$, * $p = 0.0129$). **(H)** Quantification of Western blot for total CaMKIIα. Unpaired t-test ($t = 0.8324$, $df = 15$, $p = 0.4183$). **(I)** Quantification of Western blot for total CaMKIIβ. Unpaired t-test ($t = 1.712$, $df = 15$, $p = 0.1075$).

Figure 7. Enhanced interaction of ArcKR with the ER membrane protein Calnexin. **(A-C)** Representative blots after pulldown of myc-ArcWT or myc-ArcKR and immunoblotted for the indicated tagged proteins. **(D)** Increased co-immunoprecipitation of Calnexin with ArcKR (Unpaired t-test, $p = 0.0009$).

Figure 1

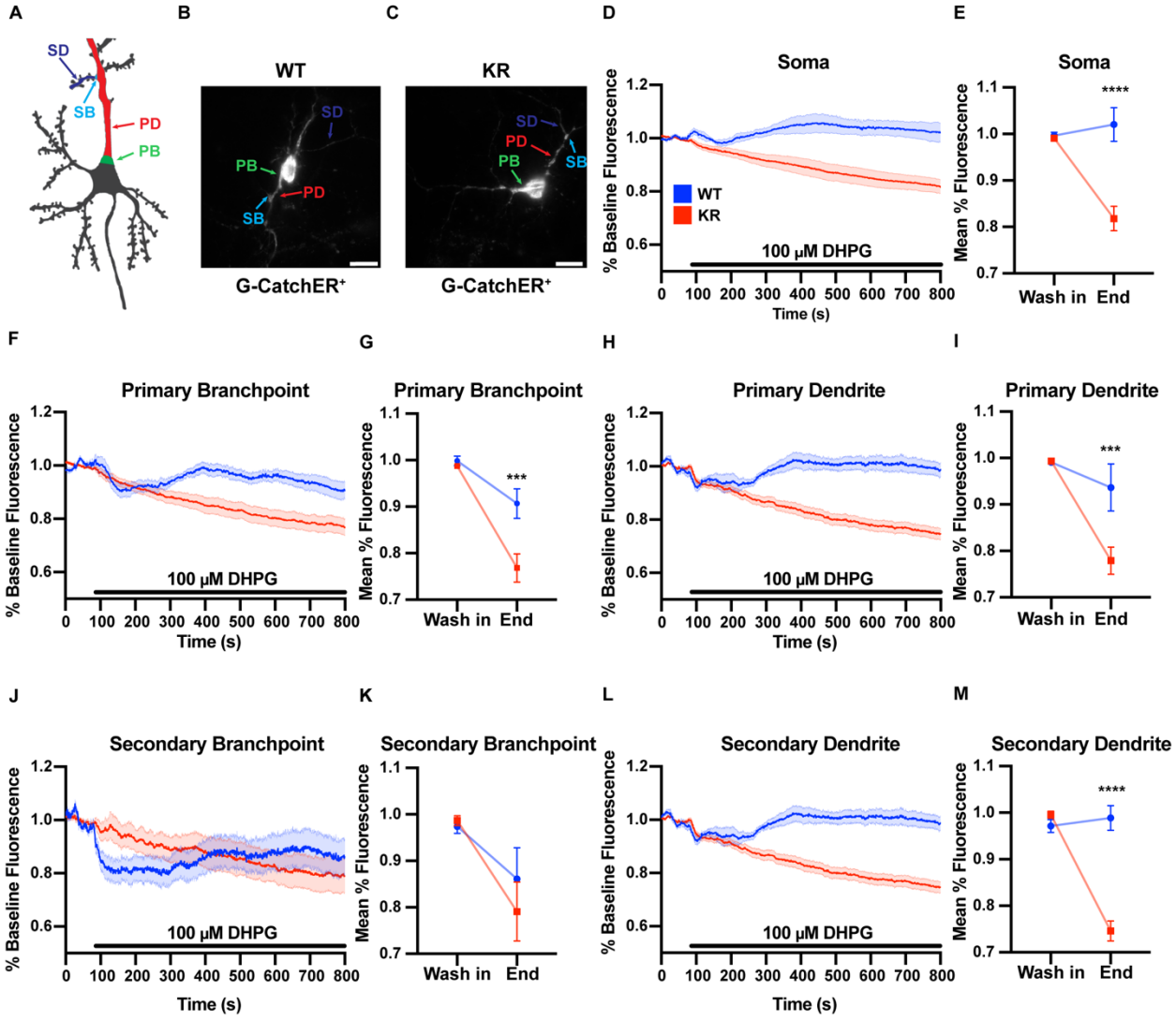
A
SD
SB
PD
PB
B
WT
SD
PB
PD
SB
G-CatchER+
C
KR
SD
PD
PB
SB
G-CatchER+
D
Soma
% Baseline Fluorescence
WT
KR
100 μM DHPG
Time (s)
E
Soma
Mean % Fluorescence
****
Wash in
End
F
Primary Branchpoint
% Baseline Fluorescence
100 μM DHPG
Time (s)
G
Primary Branchpoint
Mean % Fluorescence
***
Wash in
End
H
Primary Dendrite
% Baseline Fluorescence
100 μM DHPG
Time (s)
I
Primary Dendrite
Mean % Fluorescence
***
Wash in
End
J
Secondary Branchpoint
% Baseline Fluorescence
100 μM DHPG
Time (s)
K
Secondary Branchpoint
Mean % Fluorescence
Wash in
End
L
Secondary Dendrite
% Baseline Fluorescence
100 μM DHPG
Time (s)
M
Secondary Dendrite
Mean % Fluorescence
****
Wash in
End

Figure 2

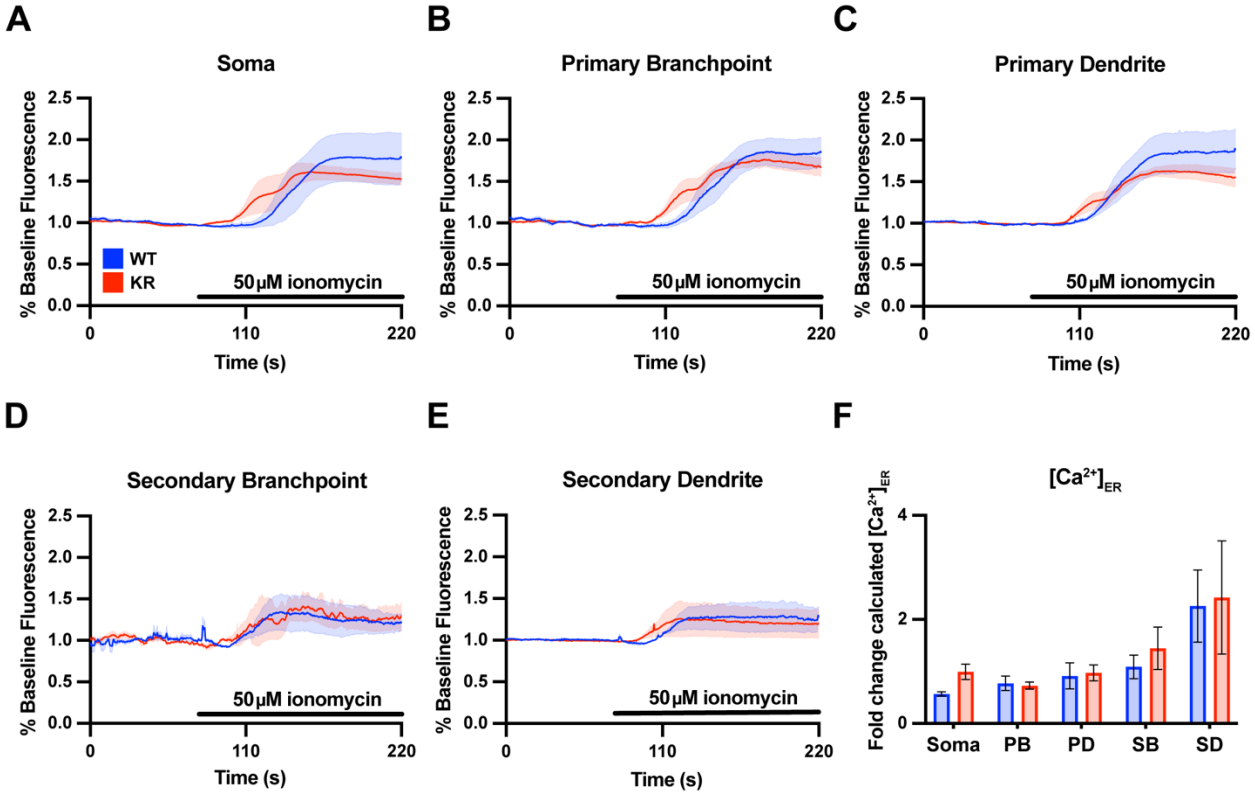
A
Soma
B
Primary Branchpoint
C
Primary Dendrite
D
Secondary Branchpoint
E
Secondary Dendrite
F
% Baseline Fluorescence
Time (s)
WT
KR
50 µM ionomycin
0
110
220
0.0
0.5
1.0
1.5
2.0
2.5
[Ca2+]ER
Fold change calculated [Ca2+]ER
Soma
PB
PD
SB
SD

Figure 3

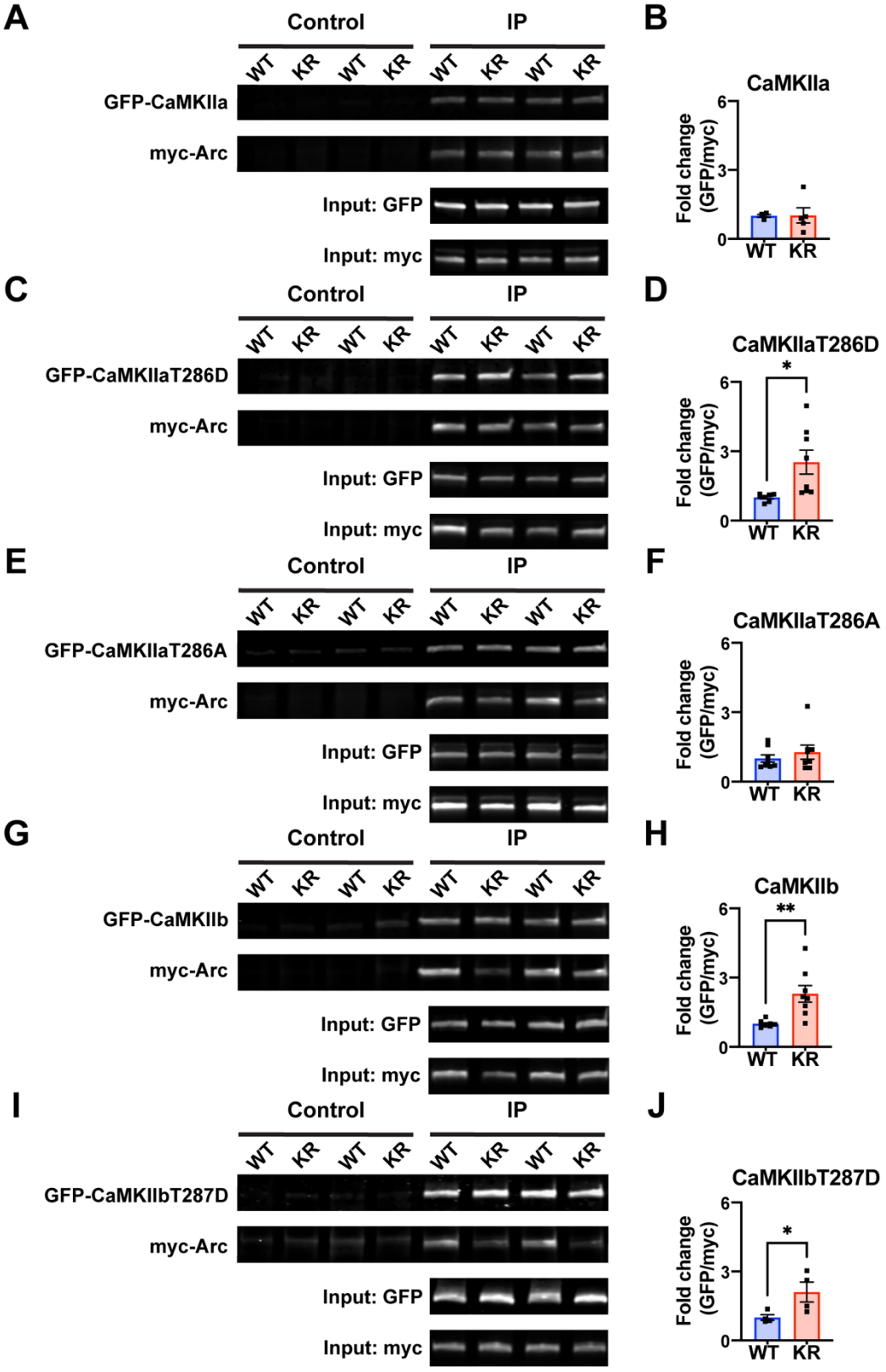
A
Control
IP
WT KR WT KR WT KR WT KR
GFP-CaMKIIa
myc-Arc
Input: GFP
Input: myc
B
CaMKIIa
Fold change (GFP/myc)
6
3
0
WT KR
C
Control
IP
WT KR WT KR WT KR WT KR
GFP-CaMKIIaT286D
myc-Arc
Input: GFP
Input: myc
D
CaMKIIaT286D
*
Fold change (GFP/myc)
6
3
0
WT KR
E
Control
IP
WT KR WT KR WT KR WT KR
GFP-CaMKIIaT286A
myc-Arc
Input: GFP
Input: myc
F
CaMKIIaT286A
Fold change (GFP/myc)
6
3
0
WT KR
G
Control
IP
WT KR WT KR WT KR WT KR
GFP-CaMKIIb
myc-Arc
Input: GFP
Input: myc
H
CaMKIIb
**
Fold change (GFP/myc)
6
3
0
WT KR
I
Control
IP
WT KR WT KR WT KR WT KR
GFP-CaMKIIbT287D
myc-Arc
Input: GFP
Input: myc
J
CaMKIIbT287D
*
Fold change (GFP/myc)
6
3
0
WT KR

Figure 4

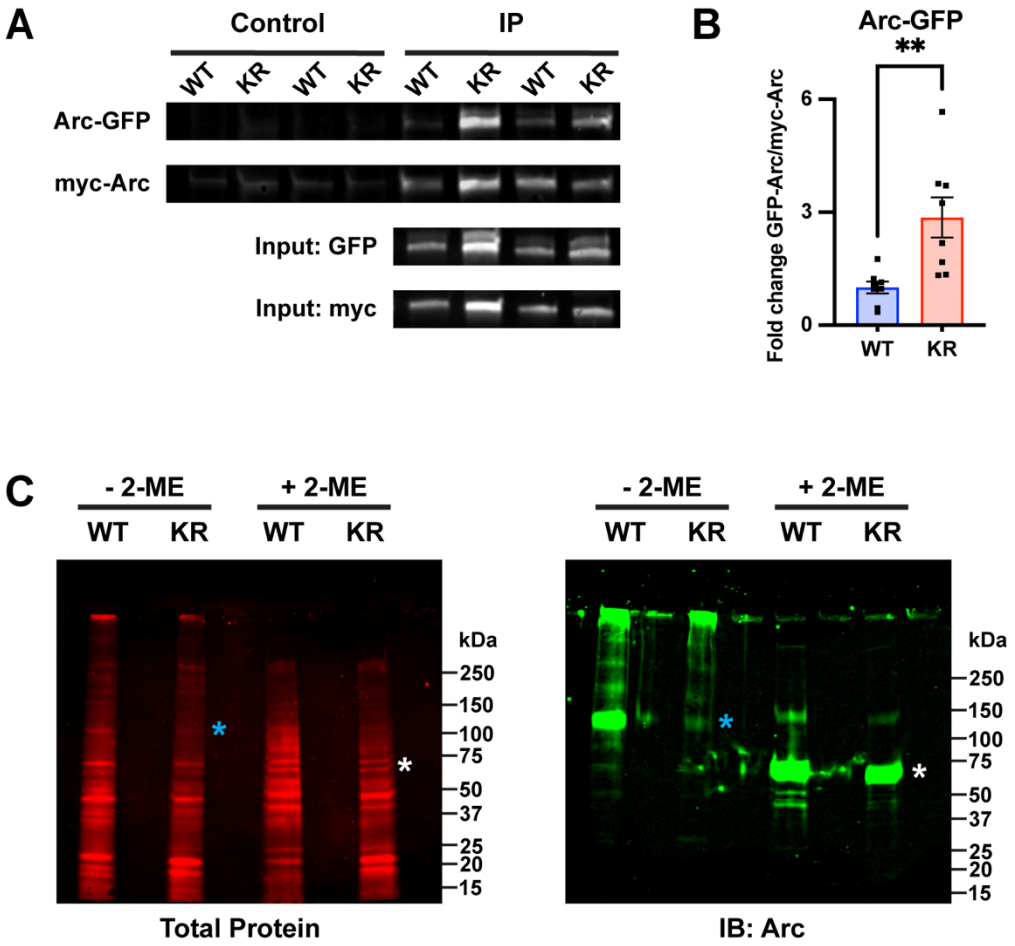
A
Control
IP
WT
KR
WT
KR
WT
KR
WT
KR
Arc-GFP
myc-Arc
Input: GFP
Input: myc
B
Arc-GFP
**
Fold change GFP-Arc/myc-Arc
6
3
0
WT
KR
C
- 2-ME
+ 2-ME
WT
KR
WT
KR
kDa
250
150
100
75
50
37
25
20
15
Total Protein
IB: Arc

Figure 5

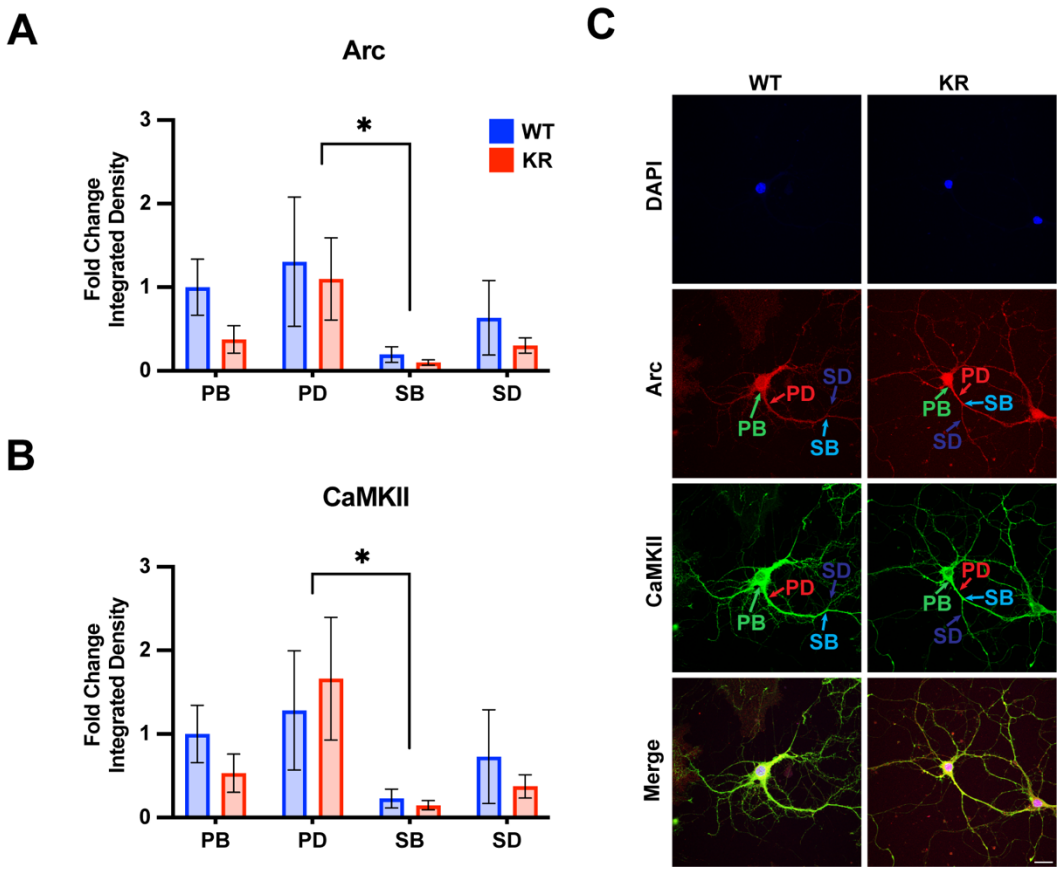
A
Arc
Fold Change
Integrated Density
3
2
1
0
*
WT
KR
PB
PD
SB
SD
B
CaMKII
Fold Change
Integrated Density
3
2
1
0
*
PB
PD
SB
SD
C
WT
KR
DAPI
Arc
CaMKII
Merge
PD
SD
PB
SB

Figure 6

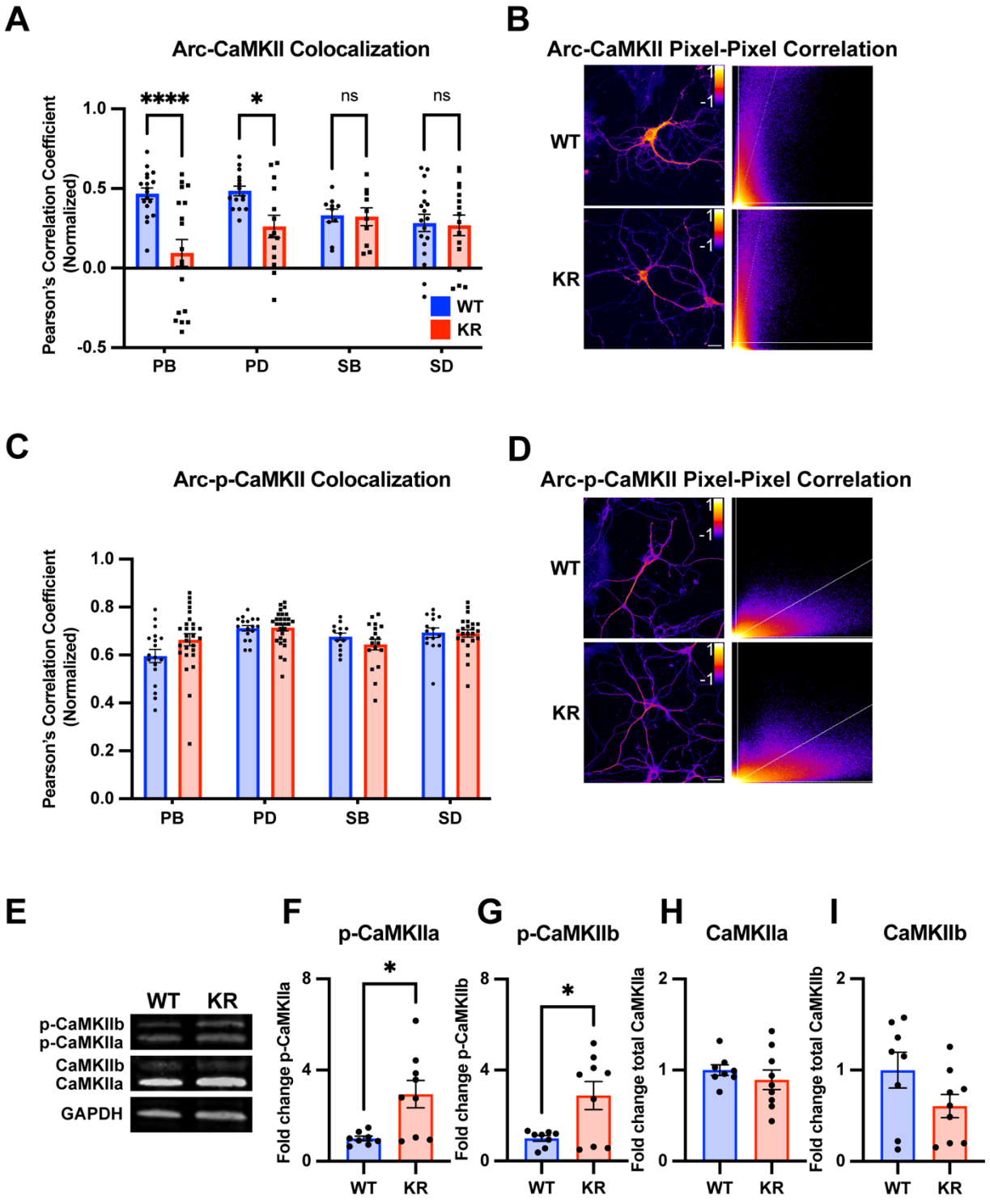
A
Arc-CaMKII Colocalization
Pearson's Correlation Coefficient (Normalized)
1.0
0.5
0.0
-0.5
****
*
ns
ns
PB
PD
SB
SD
WT
KR
B
Arc-CaMKII Pixel-Pixel Correlation
WT
KR
1
-1
C
Arc-p-CaMKII Colocalization
Pearson's Correlation Coefficient (Normalized)
1.0
0.8
0.6
0.4
0.2
0.0
PB
PD
SB
SD
D
Arc-p-CaMKII Pixel-Pixel Correlation
WT
KR
1
-1
E
WT
KR
p-CaMKIIb
p-CaMKIIa
CaMKIIb
CaMKIIa
GAPDH
F
p-CaMKIIa
Fold change p-CaMKIIa
8
4
0
*
WT
KR
G
p-CaMKIIb
Fold change p-CaMKIIb
8
4
0
*
WT
KR
H
CaMKIIa
Fold change total CaMKIIa
2
1
0
WT
KR
I
CaMKIIb
Fold change total CaMKIIb
2
1
0
WT
KR

Figure 7

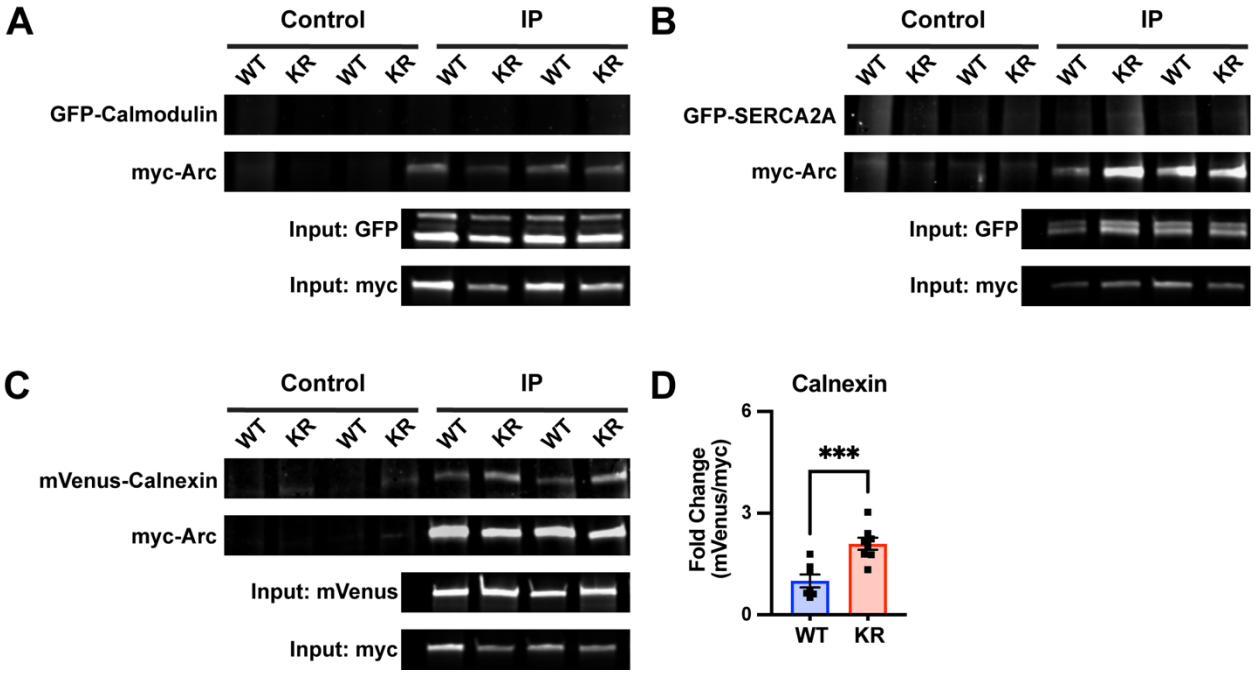
A
Control
IP
WT
KR
WT
KR
WT
KR
WT
KR
GFP-Calmodulin
myc-Arc
Input: GFP
Input: myc
B
Control
IP
WT
KR
WT
KR
WT
KR
WT
KR
GFP-SERCA2A
myc-Arc
Input: GFP
Input: myc
C
Control
IP
WT
KR
WT
KR
WT
KR
WT
KR
mVenus-Calnexin
myc-Arc
Input: mVenus
Input: myc
D
Calnexin
Fold Change
(mVenus/myc)
6
3
0
***
WT
KR